Sound speed in water-saturated glass beads as a function of frequency and porosity

Theodore F. Argo IV, Matthew D. Guild, and Preston S. Wilson[a)]
Department of Mechanical Engineering and Applied Research Laboratories, The University of Texas at Austin, P.O. Box 8029, Austin, Texas 78713-8029
targo@mail.utexas.edu, mdguild@arlut.utexas.edu, pswilson@mail.utexas.edu

Matthias Schröter
Max Planck Institute for Dynamics and Self-Organization, Bunsenstraiße 10, 37073 Gottingen, Germany
matthias.schroeter@ds.mpg.de

Charles Radin
Department of Mathematics, The University of Texas at Austin, 1 University Station, C1200, Austin, Texas 78712
radin@math.utexas.edu

Harry L. Swinney
Center for Nonlinear Dynamics and Department of Physics, The University of Texas at Austin, 1 University Station C1610, Austin, Texas 78712
swinney@chaos.utexas.edu

Abstract: Sound propagation in water-saturated granular sediments is known to depend on the sediment porosity, but few data in the literature address both the frequency and porosity dependency. To begin to address this deficiency, a fluidized bed technique was used to control the porosity of an artificial sediment composed of glass spheres of 265 μm diameter. Time-of-flight measurements and the Fourier phase technique were utilized to determine the sound speed for frequencies from 300 to 800 kHz and porosities from 0.37 to 0.43. A Biot-based model qualitatively describes the porosity dependence.

PACS numbers: 43.30.Ma, 43.35.Bf [GD]
Date Received: December 23, 2010 **Date Accepted:** December 29, 2010

1. Introduction

Numerous models have been proposed to describe sound propagation in water-saturated granular materials (see Refs. 1–5 for a sampling); however, no model yet accurately describes the sound speed in these materials across the full range of frequencies of interest in underwater acoustics. Measurements of the acoustic properties of water-saturated sediments have been made under a variety of conditions including *in situ* measurements,[6,7] retrieved samples,[7,8] reconstituted samples,[9,10] and artificial sediments.[11] There is a large variability in the observed sound speeds of these various sediments due to the wide range of porosities, permeabilities, and other physical properties they exhibit. Richardson and Jackson have studied the effect of porosity on a global scale, compiling numerous measurements obtained across many sediment types.[12] Naturally, the sediment porosity changes are also accompanied by grain size and material differences.

In none of these studies, nor in any other studies known to the authors, was the effect of porosity studied in a controlled manner across a range of frequencies, for a single sediment sample with uniform grain size distribution. In such an

[a)]Author to whom correspondence should be addressed.

idealized case, one can focus on the effect of porosity in isolation, and, with sufficient knowledge of most of the sediment physical parameters, one can make meaningful comparisons to various models of sound propagation. Toward this end, a fluidized bed apparatus was used to prepare specific porosities of a spherical glass bead sediment, and ultrasonic time-of-flight measurements were obtained. Experimental results were compared to the predictions of the Williams effective density fluid model (EDFM).[13] The purpose of this brief communication is to describe the porosity-control technique as applied to sediment acoustics and to present a set of example measurements.

2. Description of the experiment

The artificial sediment was composed of soda lime glass spheres of 265 ± 15 μm diameter saturated with degassed distilled water. The beads were sorted using a sieve shaker between 250 and 280 μm fine mesh sieves. The mass of the dry spheres was measured, and the spheres were then added to the apparatus [shown in Fig. 1(a)]. Degassed distilled water was then continuously pumped through the sample for 30 min and then allowed to rest overnight to dissolve trapped gas bubbles.

Sediment porosity β was controlled by using the fluidized bed apparatus [shown in Fig. 1(a)], which is similar to the one described by Schröter *et al.*[14] The interior of the sample holder was 6×6 cm^2 and 30 cm tall, with the sediment height dependent upon porosity, but nominally 100 mm. Two parallel polycarbonate walls of the sample holder were 1 mm thick and the opposite two were 10 mm thick. Control of the porosity of the monodisperse fluid-saturated bead pack is initiated by pumping water at a particular flow rate through the distributor (a block of sintered bronze powder, 5 mm thick with approximately 10 μm diameter pores). The beads are carried into suspension, with the overall magnitude of their motion governed by the flow rate. The beads achieve steady-state motion and after 2 min, the flow is stopped. The beads are then given 1 min to settle. The resulting porosity is dependent upon the flow rate. An additional procedure was used to achieve uniform porosity for $\beta < 0.40$: A series of flow pulses were introduced, starting at a high flow rate but with an incrementally decreasing flow rate. This procedure allowed the bead column to settle more uniformly. The spatial variability of the porosity achieved by this technique was measured using micro-computed x-ray tomograms and porosity variations of about ± 0.005 were observed.

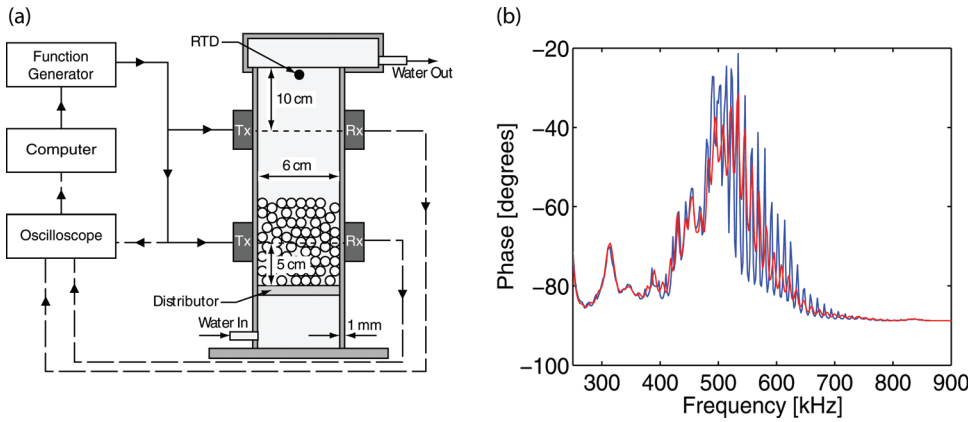

Fig. 1. (Color online) (a) A schematic diagram of the experimental apparatus. Solid (dashed) line denotes the transmitted (received) electrical signal paths. The glass beads are not drawn to scale. The phase of the measured electrical input impedance of one of the receiving transducers depicted in (a) is shown in (b). The blue curve is for the transducer mounted in the apparatus when filled with water, and the red curve is for water-saturated beads. The phase difference apparent within the experimental frequency range (300–800 kHz) leads to correctable systematic errors in the sound speed measurement.

A rectangular excitation pulse with a 10 V amplitude and a 1.25 μs width was directed to a pair of broadband ultrasonic transducers (labeled Tx) with center frequencies of 500 kHz, which transmitted simultaneously through the water and sediment paths, as shown in Fig. 1(a). Another pair of ultrasonic transducers (labeled Rx) with center frequencies of 550 kHz received the acoustic signals. Commercially available ultrasonic coupling gel was used between the transducer faces and the sample holder walls, and custom clamps were used to repeatedly locate and hold the transducers in place. Their positions were held constant during the course of the experiments. A digital storage oscilloscope acquired both the source and received signals. In all cases, 512 linear time-domain signals were averaged onboard with the scope to remove noise. The averaged signals were transferred to a computer for analysis.

To determine sediment porosity, images of the beads were obtained with a digital camera at the same time as the acoustic measurements. A fiducial scale indicating sediment height h was placed within the field of view of the camera. The porosity of the sample β was determined with $\beta = 1 - m_b/(\rho_b hA)$, where m_b and ρ_b are the dry mass and density of the beads, h is the height of the beads within the column, and A is the cross-sectional area of the column. The uncertainty in the porosity is primarily due to the uncertainty in the area and the bead density.[15] In the present experiment, this resulted in a porosity uncertainty of ± 0.003. The packing state of the sediment was found to be unaffected by the acoustic excitation. This was verified by comparing pings at the beginning, middle, and end of the acoustic averaging interval. No systematic variations in the received waveforms were found. A resistance temperature detector, labeled RTD in Fig. 1(a), was used to measure the temperature during the acoustic measurements. Equation (5.6.8) of Ref. 16 was later used to determine the sound speed c_0 of the distilled water at the experimental temperature.

The apparatus and preparation technique described above yielded porosity control but also resulted in an acoustic path length that was shorter than desired. For a fixed path length uncertainty, sound speed measurement uncertainty is inversely proportional to path length. Increasing the cross-sectional area of the apparatus while retaining uniform porosity is difficult. Since the goal of this work was to investigate the effect of porosity, we chose to achieve a homogeneous sediment at the expense of simplicity in the acoustic data analysis. In addition, the porosity-control procedure can take as long as several hours for the dense sediments. Because the water temperature follows temperature fluctuations in the laboratory, there could be significant temperature-dependent sound speed changes in the sample before and after the procedure. Hence, the four-transducer apparatus shown in Fig. 1(a) was used to facilitate contemporaneous post-preparation water path calibration and sediment path measurements.

Coupling between the sediment sample and the tank walls and transducers was found to be significant, as demonstrated in Fig. 1(b), which shows the phase of the measured electrical input impedance of one of the receiving acoustic transducers when mounted in the apparatus filled only with water, and when filled with water-saturated beads. There is as much as a 30° phase difference between these two cases. Further, initial measurements with distilled water revealed that the sound speed determined by Eq. (1) applied to the present four-transducer apparatus included a systematic error due to a small path length difference between the two transducer pairs. The effect of these systematic errors was found to be of the same order of magnitude (a few percent) as the sound speed changes as expected from the porosity dependency. Therefore, the calibration and error correction procedure described in Sec. 3 was implemented to overcome these path length and coupling-related errors. Near-field effects were quantified as described in Ref. 17 and found to be insignificant, which was also the case for a similar experiment described in Ref. 10.

3. Analysis

The fast Fourier transforms (FFTs) of the received signals for both the water paths and sediment paths were calculated. A Fourier phase technique[18] was then used to

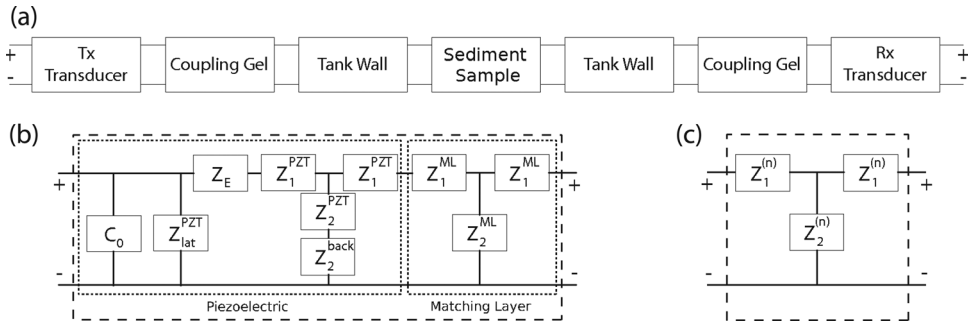

Fig. 2. (a) A schematic diagram of the transmission line model. It is composed of a Mason model for the transducers (b) and generic transmission line elements (c) for the remaining layers.

obtain a measurement of the apparent sound speed c_{sys} of the sediment within the experimental system. This sound speed was calculated with

$$c_{\text{sys}} = c_0 \left[1 - \frac{c_0 \Delta\phi}{l\omega}\right]^{-1}, \tag{1}$$

where c_0 is the sound speed in the water portion of the fluidized bed determined by Eq. (5.6.8) of Ref. 16, l is the length of travel for the acoustic wave within the sample, $\omega = 2\pi f$ is the angular frequency, and $\Delta\phi$ is the difference in phase between the two FFT spectra at frequency ω.

An equivalent circuit transmission line model of the experimental system [Fig. 2(a)] was used to correct the systematic errors described in Sec. 2. The model included the transducers, coupling gel, tank walls, and the sediment (or water). The passive layers [Fig. 2(c)] were modeled with $Z_0^{(n)} = \rho^{(n)} c^{(n)} S^{(n)}/N^2$, $Z_1^{(n)} = jZ_0^{(n)} \tan[k^{(n)} l^{(n)}/2]$, and $Z_2^{(n)} = -jZ_0^{(n)}/\sin[k^{(n)} l^{(n)}]$, where $k^{(n)}$, $\rho^{(n)}$, and $c^{(n)}$ are the wave number, density, and sound speed within the nth component respectively; $l^{(n)}$ is the path length in the nth component; $S^{(n)}$ is the surface area; and N is the transformation factor from one physical domain to another. The frequency-dependent value of the sediment sound speed used in the system model is denoted by c_{sed} and is used to construct both k and c for the sediment layer. A Mason equivalent circuit model of a thickness mode piezoelectric resonator with a matching layer[19] was used to model the transducers [Fig. 2(b)]. The unloaded electrical impedance of each transducer was measured and the values for each model element are shown in Fig. 2(b) were found by fitting the model to the impedance measurement, including the use of the properties for the piezoelectric ceramic PZT-4 listed in Table 4.3 of Ref. 20. Additional material properties for the model elements are listed in Table 1. Measurements made with distilled degassed water occupying both transmission paths allowed for calibration of the transmission path lengths in the model.

To perform the correction, the experimental input signals for the water and sediment paths were digitized, FFTs were taken, the resulting spectra were input into

Table 1. Parameters used in the transmission line model. The sound speed and density of the transducer matching layers and coupling gel were obtained from their respective manufacturers. The sample holder wall density was measured, and its sound speed was also measured using commercial ultrasonic testing instrumentation.

	Density (kg/m^3)	Sound speed (m/s)
Matching layer	1200	2650 $(1 + 0.01j)$
Coupling gel	1000	1500
Sample holder wall	1200	1800 $(1 + 0.01j)$

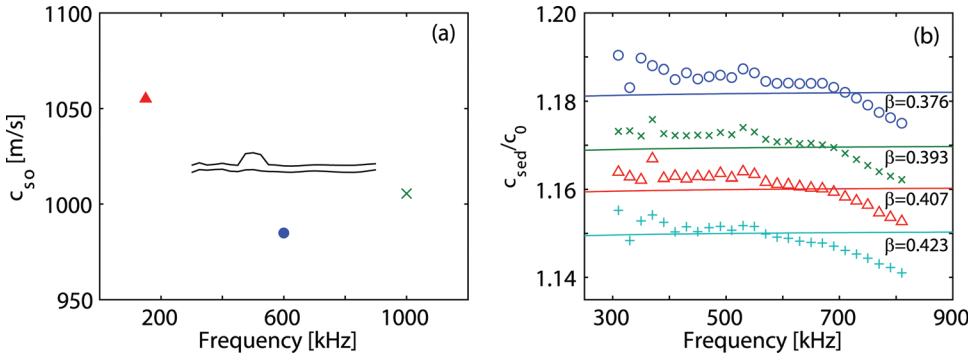

Fig. 3. (Color online) The measured sound speed for silicone oil samples are shown as a function of frequency (a). The upper and lower curves corresponds to 1×10^5 cSt silicone oil at 23.0 °C and the dashed line corresponds to 1×10^6 cSt silicone oil at 23.6 °C, respectively. The symbol (×) corresponds to the measurement of sound speed in 100 cSt silicone oil from Ref. 21, the circle corresponds to the measurement of sound speed in 1000 cSt silicone oil from Ref. 22, and the triangle corresponds to the measurement of sound speed in 1000 cSt silicone oil from Ref. 23. The literature sound speeds were extrapolated to 23.0 °C using the temperature coefficients stated in their respective references. Measured sound speed ratios of water-saturated glass beads are shown as a function of frequency in (b). Solid lines correspond to the predictions of the EDFM[13] and symbols correspond to measurements. In (b), circles correspond to a porosity of 0.376, symbols (×) correspond to a porosity of 0.393, triangles correspond to a porosity of 0.407, and plus symbols (+) correspond to a porosity of 0.423.

the system model, and the output spectra were obtained. These modeled output spectra were then subjected to the calculation described in Eq. (1) which yield a modeled system value of $c_{sys,m}$. Using Newton–Raphson iteration, c_{sed} was systematically varied in the model until the modeled system value $c_{sys,m}$ matched the measured value of c_{sys} for each frequency ω and for each porosity β. The values of c_{sed} that achieved this match were taken to be the free-field sound speed of the sediment samples and are reported in Figs. 3(b) and 4.

Imperfect knowledge of the water and sediment path lengths, known to within 0.1 mm, and total length of the other components (pzt, matching layer, coupling gel and sample holder wall), known to within 0.05 mm, were the largest source of measurement uncertainty in this work. The effect of these uncertainties was determined using the circuit model and resulted in a ±0.0015 uncertainty in sound speed ratio, which is about the same size as the data points used in Figs. 3(b) and 4.

4. Results

A calibration of the system was performed using silicone oil with viscosities of 1×10^5 and 1×10^6 cSt. The calibration was performed by adding a 10 cm thick layer of silicone fluid to the top of a 10 cm thick layer of degassed distilled water. Since silicone fluid is less dense than water and the two fluids are immiscible, stratification of the

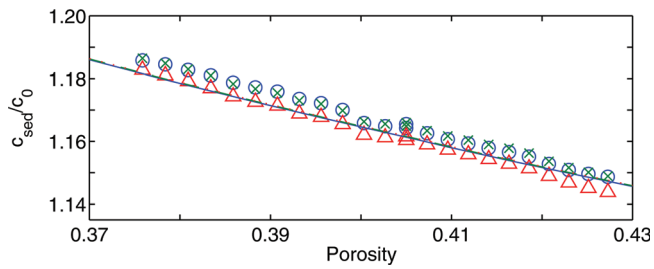

Fig. 4. (Color online) Measured sound speed ratios of water-saturated glass beads are shown as a function of porosity. Dashed and solid lines (nearly indistinguishable) correspond to the predictions of the EDFM[13] and symbols correspond to measurements. Circles correspond to a frequency of 400 kHz, symbols (×) correspond to a frequency of 550 kHz, and triangles correspond to a frequency of 700 kHz.

Table 2. Parameters used as inputs to the Williams EDFM model.[13] Grain density was measured using a Gay–Lussac flask. Water sound speed was given by Eq. (5.6.8) in Ref. 15. Tortuosity was calculated using Ref. 24 with an exponent of 0.5. Permeability was calculated using the Kozeny–Carman Equation[25] with a coefficient of 5 and the pore size factor given by Ref. 13. Bead bulk modulus was taken from the manufacturer's specification. Porosity was determined by the method in Sec. 2. When multiple entries appear within a cell, they are for the four porosities that are tabulated here, respectively, and that also appear in Fig. 3(b).

Grain density	2487 ± 1 kg/m^3	Water density	998 kg/m^3
Bead bulk modulus	41.175 GPa	Water sound velocity (m/s)	1474, 1472, 1471, 1472
Water viscosity	0.001 Pas	Permeability (m^{-2})	$(5.32, 6.44, 7.50, 8.87) \times 10^{-11}$
Tortuosity	1.63, 1.59, 1.57, 1.54	Porosity	0.376, 0.393, 0.407, 0.423

fluids was achieved. Sound speeds were calculated using Eq. (1) and processed using the model outlined in Sec. 3. The resulting silicone oil sound speeds, c_{so}, are shown in Fig. 3(a) and fall within a range of values found in the literature.[21–23]

In Fig. 3(b), the frequency dependence of the measured sediment sound speed c_{sed} is compared to the predictions of the EDFM,[13] for the parameters given in Table 2. Negative dispersion is apparent in Fig. 3(b) for all porosities above 550 kHz. Considering just one frequency, say 600 kHz, the variation in the measured sound speed as a function of porosity is well-predicted by the EDFM.

In Fig. 4, the porosity dependence of the measured sound speed is shown and compared to the predictions of the EDFM at three frequencies. Measurements at porosities not shown in Fig. 3(b) are shown here. It is apparent that the EDFM does a good job of describing the observed relative porosity dependence. Note that all the sound speeds predicted by the EDFM nearly collapse onto a single line. The negative dispersion exhibited by the measured sound speed remains apparent. Plotted this way, the sound speed monotonically decreases with porosity. Therefore, the porosity appears to be a good indicator of the sound speed in this glass bead sediment.

5. Conclusion

The porosity- and frequency-dependent sound speed in an artificial water-saturated glass bead sediment was measured using a fluidized bed apparatus with a time-of-flight acoustic measurement and a Fourier phase technique. The relative dependence of the sound speed on porosity is properly predicted by the Biot-based EDFM model throughout the experimental frequency range, 300–800 kHz, and it also quantitatively described the sound speed ratio to within $\pm 1\%$. The measured frequency dependence reveals negative dispersion at frequencies above 550 kHz. The authors acknowledge that other models that address multiple scattering[2] and high-frequency viscosity effects[26] will likely do a better job predicting the dispersion in this frequency range. The present purpose is to report the porosity-control technique and initial measurements obtained with it and not to identify the physical cause of the observed dispersion. The reported measurement and data analysis techniques are similar to those reported in Refs. 2 and 10 in which negative dispersion was also observed. All these techniques are variations of the common immersion technique and there is no evidence indicating that the determination of sound speed with these techniques is dependent on the physical nature or origin of the dispersion. Measurements with various bead sizes and natural sand grains as well as a more thorough model evaluation are currently underway.

Acknowledgments

This work was supported by the Office of Naval Research Ocean Acoustics, the Robert A. Welch Foundation Grant F-0805, and National Science Foundation Grant DMS-0700120. The authors also wish to acknowledge Nicholas P. Chotiros for insightful discussions and Udo Krafft for experimental support.

References and links

[1]M. A. Biot, "Generalized theory of acoustic propagation in porous dissipative media," J. Acoust. Soc. Am. **34**, 1254–1264 (1962).

[2]L. Schwartz and T. J. Plona, "Ultrasonic propagation in close-packed disordered suspensions," J. Appl. Phys. **55**, 3971–3977 (1984).

[3]R. D. Stoll, *Sediment Acoustics* (Springer-Verlag, New York, 1989) pp. 5–20.

[4]M. J. Buckingham, "Theory of compressional and shear waves in fluidlike marine sediments," J. Acoust. Soc. Am. **103**, 288–299 (1998).

[5]N. P. Chotiros and M. J. Isakson, "A broadband model of sandy ocean sediments: Biot-Stoll with contact squirt flow and shear drag," J. Acoust. Soc. Am. **116**, 2011–2022 (2004).

[6]A. Turgut and T. Yamamoto, "Measurements of acoustic wave velocities and attenuation in marine sediments," J. Acoust. Soc. Am. **87**, 2376–2383 (1990).

[7]K. L. Williams, D. R. Jackson, E. I. Thorsos, D. Tang, and S. G. Schock, "Comparison of sound speed and attenuation measured in a sandy sediment to predictions based on the Biot theory of porous media," IEEE J. Ocean. Eng. **27**, 413–428 (2002).

[8]E. L. Hamilton and R. T. Bachman, "Sound velocity and related properties of marine sediments," J. Acoust. Soc. Am. **72**, 1891–1904 (1982).

[9]D. J. Shirley and L. D. Hampton, "Shear-wave measurements in laboratory sediments," J. Acoust. Soc. Am. **63**, 607–613 (1978).

[10]K. I. Lee, V. F. Humphrey, B.-N. Kim, and S. W. Yoon, "Frequency dependencies of phase velocity and attenuation coefficient in a water-saturated sandy sediment from 0.3 to 1.0 MHz," J. Acoust. Soc. Am. **121**, 2553–2558 (2007).

[11]B. T. Hefner and K. L. Williams, "Sound speed and attenuation measurements in unconsolidated glass-bead sediments saturated with viscous pore fluids," J. Acoust. Soc. Am. **120**, 2538–2549 (2006).

[12]D. R. Jackson and M. D. Richardson, *High Frequency Seafloor Acoustics* (Springer Science, New York, 2007) pp. 125–151.

[13]K. L. Williams, "An effective density fluid model for acoustic propagation in sediments derived from Biot theory," J. Acoust. Soc. Am. **110**, 2276–2281 (2001).

[14]M. Schröter, S. Nägle, C. Radin, and H. L. Swinney, "Phase transition in a static granular system," Europhys. Lett. **78**, 44004 (2007).

[15]M. Schröter, D. I. Goldman, and H. L. Swinney, "Stationary state fluctuations in a granular medium," Phys. Rev. E **71**, 030301(R) (2005).

[16]L. E. Kinsler, A. R. Frey, A. B. Coppens, and J. V. Sanders, *Fundamentals of Acoustics,* 4th ed. (Wiley, New York, 1999) p. 121.

[17]W. Xu and J. J. Kaufman, "Diffraction correction methods for insertion ultrasound attenuation estimation," IEEE Trans. Biomed. Eng. **40**, 563–570 (1993).

[18]J. B. Molyneux and D. R. Schmitt, "Compressional-wave velocities in attenuating media: A laboratory physical model study," Geophysics **65**, 1162–1167 (2000).

[19]W. P. Mason, *Physical Acoustics and the Properties of Solids* (Van Nostrand, Princeton, NJ, 1958) pp. 51–86.

[20]O. B. Wilson, *Introduction to the Theory and Design of Sonar Transducers* (Peninsula, Los Altos, California, 1988) pp. 74–75.

[21]B. Hartmann and J. Jarzynski, "Immersion apparatus for ultrasonic measurements in polymers," J. Acoust. Soc. Am. **56**, 1469–1477 (1974).

[22]A. Weissler, "Ultrasonic investigation of molecular properties of liquids. III. Linear polymethylsiloxanes," J. Am. Chem. Soc **71**, 93–95 (1949).

[23]R. N. Capps, C. M. Thompson, and F. J. Weber, "Handbook of sonar transducer passive materials," NRL Memorandum Report No. 4311, Naval Research Laboratory (1981).

[24]R. Dias, J. A. Teixeira, M. Mota, and A. Yelshin, "Tortuosity variation in a low density binary particulate bed," Sep. Purif. Technol. **51**, 180–184 (2006).

[25]V. Batu, *Aquifer Hydraulics: A Comprehensive Guide to Hydrogeologic Data Analysis* (Wiley-IEEE, Hoboken, NJ, 1998) p. 42.

[26]N. P. Chotiros and M. J. Isakson, "High-frequency dispersion from viscous drag at the grain-grain contact in water-saturated sand," J. Acoust. Soc. Am. Express Lett. **124**, EL296–EL301 (2008).